Propagating Thermal Vortex-Ring As a Generalization of Hill's Vortex

Jun–ichi Yano, Glenn Flierl

Geophysical and Astrophysical Fluid Dynamics
Vol. 00, No. 00, 00 Month 2012, 1–26

Propagating Thermal Vortex-Ring As a Generalization of Hill's Vortex

Jun-Ichi Yano†* and Glenn R. Flierl‡

†CNRM UMR3589 (CNRS), Météo-France, 31057 Toulouse Cedex, France
‡Department of Earth, Atmospheric and Planetary Sciences, Massachusetts Institute of Technology, Cambridge, Massachusetts

(*Received 00 Month 20xx; final version received 00 Month 20xx*)

An analytical solution of the thermal vortex ring in the similarity regime is derived in this study. An attempt is first made to find a steadily-propagating solution as an extension of the Hill's vortex by considering its modification by buoyancy. However, the derived solution is incomplete, because the internal and external solutions cannot match properly. Unsteadiness of the system due to the presence of buoyancy removes this inconsistency. Separating dependencies in time and space leads to a temporal tendency of the vortex-ring radius proportional to $t^{1/2}$ with t the time, as expected from the similarity solution. Modifications to the spatial dependency are relatively minor compared to the original steadily-propagating solution. The analytical solution overall reproduces the basic characteristics of thermal vortex rings found in recent numerical simulations, especially a negative dynamic drag, albeit in a very qualitative manner.

DOC/convection/ring/modon/ms.tex, 14 December 2024

1. Introduction

The vortex ring is an axisymmetric doughnut-shaped vortex, constituting a vortex pair in the vertical section, like the rings produced by a smoker. It can be studied in the laboratory by mechanically generating it in a similar manner. Alternatively, a vortex ring can be generated ejecting an isolated buoyancy anomaly. This latter type, a thermal vortex ring, is the theme of this paper.

Mechanically-generated vortex rings are more straightforward to study theoretically because they can be described purely in terms of the vortex dynamics in the inviscid limit, a limit that is also adopted in this work. As a result, it is also much easier to describe their steady propagation, and hence various theoretical solutions are also available. The best known is an analytical solution derived by Hill (1894) for a vortex ring filling a sphere. An alternative solution is obtained by taking an opposite limit of assuming that the vorticity is found only on a particular circle around a vertical axis; the solution for this vortex circle is presented in Lamb (1932). The vortex-circle solution can further be improved by including a contribution of a small, but finite, size of the vortex-ring core around the circle (*e.g.*, Hicks 1884, Sullivan *et al.* 2008). Other versions replace Hill's vortex by a "fat" vortex ring almost touching a sphere (*e.g.*, Frankel 1972, Norbury 1972). As a synthesis of these two approaches, Norbury's (1973) iterative procedure derives a family of steadily propagating solutions with any arbitrary size of vortex-ring core. However, these more general approaches than Hill's solution do not provide closed analytical forms for the solutions.

*Corresponding author. Email: jun-ichi.yano@cnrs.fr

These approaches for "inertial" vortex rings can also be applied to a category of thermal vortex rings, the so-called bubbles, because they are generated by injecting a lighter fluid into a working fluid (typically air into water). Thus, the system takes a form of two fluids with two different densities. Walters and Davidson (1963) consider the initial formation process of a bubble by a series of Legendre polynomials. Pedley (1968) analytically derives a similarity solution by Turner (1957) by considering a limit of small vortex core. Lundgren and Mansour (1991) consider a modification to Hicks' (1884) solution by buoyancy. However, a major difficulty with the bubble dynamics is its inherently unsteady behaviour, which is best described by a contour-dynamics method (Chang and Llewellyn Smith 2018, 2020).

The purpose of this study is to extend these existing studies of "inertial" vortex rings as well as bubbles to thermal vortex rings. The thermal vortex ring, or simply, thermal, has long been considered an important building block of atmospheric convection (*cf.*, Yano 2014). Indeed, there is renewed interest in the problem of thermal vortex rings, thanks to improvements of our capacity for both numerical computations (Sherwood *et al.* 2013, Romps and Charn 2015, Hernandez-Deckers and Sherwood 2016, Morrison and Peters 2018, Tarshish *et al.* 2018, Anders *et al.* 2019, Lecoanet and Jeevanjee 2019, McKim *et al.* 2020, Morrison *et al.* 2022) and laboratory experiments (Zhao *et al.* 2013, Lai *et al.* 2015, Vasel-Be-Hagh *et al.* 2015). Among the recent studies, we specifically refer to Morrison *et al.* (2022: hereafter MJY) to compare with the results of this study.

The basic strategy of this study is to extend the Hill's vortex solution to a buoyant case. As the case with Hill's vortex ring, the focus will be initially on steadily propagating solutions with no azimuthal dependence, but with a modification of the vortex-ring size due to the presence of buoyancy. In laboratory and numerical experiments, such a state is established after a transient formation of a vortex ring from an initial isolated buoyant anomaly with a quiescent state. From a theoretical point of view, this state has been investigated under the framework of a similarity theory (Scorer 1957, Turner 1957). The basic motivation of this study is to derive analytical solutions of thermal vortex rings, albeit under approximations.

For this purpose, we invoke a strongly nonlinear theory of the vortices, called the modons, as reviewed by Flierl (1987). Under this framework, the Hill's solution is obtained by assuming a homogeneous potential vorticity anomaly inside the vortex-ring core. In the next section, where a basic formulation is introduced, the effect of the buoyancy is included into this framework by generalising the potential vorticity.

The first important aspect of this generalisation is that the presence of the buoyancy no longer permits a perfectly spherical vortex ring as the case for Hill's solution. Consequently, the shape of the vortex ring, characterised by its radius, R, must also be determined as a function of the angle from the vertical axis of the vortex ring, θ, as a *free boundary* in Sec. 2. A general closed analytical expression for steadily-propagating solutions can, indeed, be derived inside and outside the spherical vortex-ring boundary, but only separately: they cannot be connected continuously over the spherical boundary. This problem is *initially* solved by assuming a constant radius, R_0, to the leading order, and the deviation of the radius, R, from this basic state is treated as a "perturbation". More precisely, the deformation of the boundary is expressed by expanding the vortex-ring radius as a power series in $\cos\theta$, where θ is the angle from the vertical axis of the vortex ring. Now, a consistent solution can be obtained but only up to $O(\cos^2\theta)$ (Sec. 2.5).

Physically speaking, a purely steadily propagating solution, pursued in Sec. 2, is not possible due to the presence of nonvanishing buoyancy in the domain average, which accelerates the thermal as a whole upwards with time. For this reason, an explicit time dependence is introduced under the separation of variables in Sec. 3 so that the unsteady tendency of the evolution can be taken into account. The time dependence reduces to a question of an expansion of the vortex ring, whereas its spatial dependence can still be determined by similar equations. Thus, the full unsteady solution can be derived simply with additional terms added

to the original steadily-propagating solution.

The analytical results obtained in Sec. 3 are compared with the existing numerical experiments, notably, by MJY in Sec. 4. Here, we specifically refer to their higher-resolution run (HIGHRES case) to compare it with our analytical results. The choice is made based on our judgment that this run with a high spatial resolution is closest to the inviscid limit in this study. Their lower-resolution run as well as other recent numerical experiments contain more significant dissipation in the momentum equation either numerically or physically. Here, we choose to compare the results in terms of the momentum budget, because it is a more commonly-accepted approach to describe the dynamics of thermal vortex rings. We refer especially to the recent efforts by Morrison (2016a, b), and Morrison and Peters (2018).

To perform the comparisons, we need to keep in mind certain caveats. First, this theoretical study focuses on the similarity regime, in which the vortex ring propagates steadily with time keeping overall the same shape, albeit with a growing tendency of the size due to the buoyancy. In numerical experiments, which are typically initiated with an isolated buoyancy anomaly with a quiescent state, this state is realised only after an initial transient evolution. Thus, the comparisons exclusively focus on the later stage of those simulations, when a similarity condition is expected to be satisfied.

Second, the analytical results obtained in this study are under the axisymmetric assumption, whereas all those numerical experiments were performed with fully three-dimensional configurations. We expect that comparisons are useful to a good extent, because those numerically-simulated vortex rings are predominantly axisymmetric, although the presence of azimuthal flows is hardly negligible. The vorticity-budget analysis of the HIGHRES run performed by a separate study (Yano and Morrison 2024) supports this expectation.

Nevertheless, it is also likely that this study with the axisymmetric assumption in the inviscid limit involves various implicit assumptions. For example, a quasi-steady assumption of the model under the separation of variables could fail if a thermal tries to pinch off on the centreline, or at least develop a point where the boundary is no longer smooth. Furthermore, the unsteady solutions are derived under relatively severe limits. First, a nonlinear unsteady effect is neglected, expecting the modification to be relatively minor. Second, the solution is derived under a severe truncation in Taylor expansion. Nevertheless, in spite of those limitations, remarkably, the obtained unsteady solution reproduces the negative dynamic pressure drag, albeit in a very crude manner, found in the numerical simulation by MJY.

2. Steadily-Propagating Solution

2.1. *Formulation*

We adopt the Boussinesq approximation with cylindrical coordinates (s, φ, z), with velocities (v_s, v_φ, v_z), but also occasionally refer to the spherical coordinates (r, θ, φ). Axisymmetry is assumed throughout, dropping the φ-dependence in the following. As a result, the vorticity has only an azimuthal component $\zeta \equiv \boldsymbol{\zeta} \cdot \hat{\boldsymbol{\varphi}} = \partial v_s/\partial z - \partial v_z/\partial s$. This is not conserved since vortex tubes will be stretched as they move radially. This point is seen more directly by realising that the azimuthal coordinate, φ, acts as a passive scalar, because there is no flow in the azimuthal direction. Thus, with application of Ertel's theorem, $\boldsymbol{\zeta} \cdot \nabla\varphi = \zeta/s$ is conserved in absence of buoyancy, and:

$$\left(\frac{\partial}{\partial t} + v_s \frac{\partial}{\partial s} + v_z \frac{\partial}{\partial z} \right) q = -\frac{1}{s} \frac{\partial b}{\partial s}. \tag{1a}$$

Here, $q = \zeta/s$ plays an analogous role to the potential vorticity in the shallow water system, because the vortex tube stretches as the radius, s, of the vortex-tube circle increases, and *vice versa*. However, under the presence of the buoyancy, this quantity, q, is no longer conserved,

as seen on the right-hand side. Thus, it merely plays a role of "relative potential vorticity", as a part of the total potential vorticity to be defined below by Eq. (7b). The equation for the buoyancy is:

$$\left(\frac{\partial}{\partial t}+v_s\frac{\partial}{\partial s}+v_z\frac{\partial}{\partial z}\right)b=0, \tag{1b}$$

assuming there is no buoyancy source to this system.

2.2. *Steady Propagation Problem*

For now, we seek a steadily propagating solution with velocity, c, upwards. The time derivatives can be absorbed into the vertical derivatives by transforming the vertical coordinate and the vertical velocity by:

$$z=z'-ct,$$
$$v_z=v_z'-c.$$

After removing the primes from the transformed variables, Eqs. (1a, b) reduce to

$$\left(v_s\frac{\partial}{\partial s}+v_z\frac{\partial}{\partial z}\right)q=-\frac{1}{s}\frac{\partial b}{\partial s}, \tag{2a}$$

$$\left(v_s\frac{\partial}{\partial s}+v_z\frac{\partial}{\partial z}\right)b=0. \tag{2b}$$

By adopting a moving coordinate, the system asymptotically tends to a homogeneous vertical flow downwards at large distances, thus

$$v_z\to -c \tag{3a}$$

$$v_s\to 0 \tag{3b}$$

as $z\to\pm\infty$. Eqs. (2a, b) are the basic set of equations to be considered until the end of Sec. 2.

A streamfunction, ψ, can be introduced by:

$$v_z=-\frac{1}{s}\frac{\partial\psi}{\partial s}, \tag{4a}$$

$$v_s=\frac{1}{s}\frac{\partial\psi}{\partial z}, \tag{4b}$$

and the potential vorticity is given by

$$q\equiv\frac{\zeta}{s}=\frac{1}{s}\left(\frac{\partial}{\partial s}\frac{1}{s}\frac{\partial}{\partial s}+\frac{1}{s}\frac{\partial^2}{\partial z^2}\right)\psi. \tag{4c}$$

With the help of the definition of streamfunction (Eqs. 4a, b), Eqs. (2a, b) further reduce to:

$$J(q,\psi)=-\frac{1}{s}\frac{\partial b}{\partial s}, \tag{5a}$$

$$J(b,\psi)=0, \tag{5b}$$

where J is the Jacobian defined by

$$J(a,b)=\frac{1}{s}\left(\frac{\partial a}{\partial s}\frac{\partial b}{\partial z}-\frac{\partial a}{\partial z}\frac{\partial b}{\partial s}\right).$$

The boundary conditions (3a,b) also reduce to:

$$\psi(s, z \to \pm\infty) \to \frac{1}{2} c s^2. \tag{5c}$$

It immediately follows from Eq. (5b) that a general solution for the buoyancy, b, is given by

$$b = \mathcal{F}(\psi),$$

in terms of a functional, $\mathcal{F}$, of ψ. In the following, we adopt a linear approximation of the general form above by setting,

$$b = -\alpha\psi, \tag{6}$$

inside the vortex ring ($r \leq R$), and set $b = 0$ in the exterior ($r > R$). Here, α is a positive definite constant, and an arbitrary constant for the streamfunction at the vortex-ring boundary is set zero. The sign convention for α is chosen from an anticipation that a positive vorticity corresponds to a positive buoyancy.

From a physical point of view, the parameter, α, can be called the buoyancy parameter, because $1/\alpha$ measures the efficiency of the buoyancy in maintaining a steady flow, with the latter measured by the streamfunction. In the present study, this "efficiency" parameter, $1/\alpha$, remains an undetermined free parameter. We believe that it depends on an initial condition of a problem, and is determined as a consequence of an initial transient evolution, that leads to a final similarity solution. We only focus on the latter aspect in the present study. It will also be shown immediately below that the buoyancy parameter, α, can also be understood in analogy with the β parameter in the quasi-geostrophic system.

We expect that this simplification (Eq. 6) can qualitatively represent more general cases, in which α depends on ψ: Eq. (6) suggests that, in general, the differential buoyancy forcing, $-\partial b/\partial s$, is re-interpreted as a generation of the potential vorticity by a downward flow (*i.e.*, $v_z < 0$), because $-\partial b/\partial s = \alpha \partial\psi/\partial s = -\alpha v_z$.

By substituting Eq. (6) into Eq. (5a):

$$J(Q, \psi) = 0, \tag{7a}$$

where Q is considered a "total" potential vorticity of this system, defined by

$$Q = q + \alpha z. \tag{7b}$$

for inside the vortex ring ($r \leq R$), and $Q = q$ in the exterior ($r > R$). Note that the parameter α in the above definition can be interpreted in analogy with the β parameter in the quasi-geostrophic potential vorticity with the vertical direction taking the role of the latitude (*cf.*, Pedlosky 1987). Although this analogy with quasi-geostrophy is drawn under a steady assumption, it will be seen later in Sec. 3 that it remains relevant for an unsteady problem.

In the following, we focus on a potential-vorticity patch of the form

$$Q = \begin{cases} Q_0 & r \leq R \\ 0 & r > R, \end{cases} \tag{8}$$

where $Q_0 > 0$ is a constant. Under this formulation, the boundary, R, remains arbitrary and must be determined by consistency.

By substituting the expression (8) into the definition of Q (7b), we find:

$$\zeta = \begin{cases} Q_0\, s - \alpha s z, & r \leq R, \\ 0, & r > R. \end{cases} \tag{9}$$

By further substituting Eq. (9) into the definition of the vorticity (4c), the problem to solve

reduces to

$$\left(\frac{\partial}{\partial s}\frac{1}{s}\frac{\partial}{\partial s}+\frac{1}{s}\frac{\partial^2}{\partial z^2}\right)\psi=\begin{cases}Q_0\,s-\alpha sz, & r\le R,\\ 0, & r>R.\end{cases} \tag{10}$$

We divide the above problem into the two components by setting $\psi=\bar{\psi}+\psi'$, which satisfy

$$\left(\frac{\partial}{\partial s}\frac{1}{s}\frac{\partial}{\partial s}+\frac{1}{s}\frac{\partial^2}{\partial z^2}\right)\bar{\psi}=\begin{cases}Q_0\,s & r\le R\\ 0 & r>R,\end{cases} \tag{11a}$$

$$\left(\frac{\partial}{\partial s}\frac{1}{s}\frac{\partial}{\partial s}+\frac{1}{s}\frac{\partial^2}{\partial z^2}\right)\psi'=\begin{cases}-\alpha sz & r\le R\\ 0 & r>R.\end{cases} \tag{11b}$$

In the following, we designate the components with $\bar{\psi}$ and ψ', respectively, the leading order and the perturbation, because formally, they are obtained by the leading order and the first order in expansion in terms of α. However, we also emphasise that the smallness of α is not assumed when deriving the perturbation solution in this section.

To obtain the solutions for Eqs. (11a, b), the following differential relation becomes useful:

$$\left(\frac{\partial}{\partial s}\frac{1}{s}\frac{\partial}{\partial s}+\frac{1}{s}\frac{\partial^2}{\partial z^2}\right)s^l z^m r^n=[l(l-2)z^2+m(m-1)s^2]s^{l-3}z^{m-2}r^n+n[2(l+m)+n-1]s^{l-1}z^m r^{n-2}. \tag{12}$$

This is proved by recalling that $r^2=s^2+z^2$, $\partial r/\partial s=s/r$, and $\partial r/\partial z=z/r$.

2.3. *Leading-Order Solution*

The leading-order solution, $\bar{\psi}$, corresponds to the classical solution of Hill's vortex. We pose the condition of vanishing streamfunction at $r=R_0$, setting $R=R_0$ in Eqs. (9), (10), and (11a, b) *tentatively*. Recall that the boundary condition at infinity is given by Eq. (5c). Under these conditions, with the help of Eq. (12), we find the leading-order solution

$$\bar{\psi}=\begin{cases}\dfrac{A}{2}s^2(R_0^2-r^2),\\ \dfrac{c}{2}s^2\left(1-\dfrac{R_0^3}{r^3}\right),\end{cases}\quad \bar{v}_s=\begin{cases}-Asz,\\ \dfrac{3c}{2}\dfrac{R_0^3}{r^5}sz,\end{cases}\quad \bar{v}_z=\begin{cases}-A(R_0^2-r^2-s^2), & r\le R_0,\\ c\left[\dfrac{R_0^3}{r^3}\left(1-\dfrac{3s^2}{2r^2}\right)-1\right], & r>R_0.\end{cases} \tag{13a, b, c}$$

A relation between the two constants, A and c, is found by continuity of the velocity at $r=R_0$, so $A=-3c/2R_0^2$. Recall that c is the propagation speed of the vortex ring, which is determined from the vorticity intensity, Q_0, and

$$c=2Q_0R_0^2/15. \tag{14}$$

2.4. *Buoyancy Contribution*

The perturbation solution, ψ', for Eq. (11b) is derived for the interior and exterior, respectively. As for the leading-order solution, we assume a spherical vortex ring for now. With the help of Eq. (12), we find that an inhomogeneous solution with the inhomogeneous term, sz, is obtained by setting $l=2$, $m=1$, and $n=2$. We also add a homogeneous solution with $l=2$, $m=1$, and $n=0$ so that the boundary condition at $r=R_0$, $\psi'=0$, is satisfied. Thus:

$$\psi'=\frac{\alpha}{14}s^2z(R_0^2-r^2),\quad v_s'=\frac{\alpha s}{14}(R_0^2-r^2-2z^2),\quad v_z'=-\frac{\alpha z}{7}(R_0^2-r^2-s^2) \tag{15a, b, c}$$

for $r\le R_0$.

The solution (15a, b, c) can be extended to the exterior ($r > R_0$) using the condition of continuity to yield:

$$\psi' = \beta s^2 z \left[1 - (\frac{R_0}{r})^5\right] R_0^2, \quad v_s' = \beta R_0^2 s \left[1 - (\frac{R_0}{r})^5 + \frac{5R_0^5 z^2}{r^7}\right], \quad v_z' = -2\beta R_0^2 z \left[1 - (\frac{R_0}{r})^5 + \frac{5R_0^5 s^2}{2r^7}\right]. \tag{16a, b, c}$$

with $\beta = -\alpha/35$. However, this solution has a problem, because the vertical velocity increases linearly with z to infinity, *i.e.*, as $z \to \pm\infty$, $v_z' \to -\beta z$. Thus, to remove this singularity at infinity, we need to subtract $\beta s^2 z$ from the streamfunction of both interior and exterior:

$$\psi' = \begin{cases} \alpha s^2 z \left(\dfrac{R^2}{10} - \dfrac{r^2}{14}\right) \\ -\beta s^2 z \left(\dfrac{R}{r}\right)^5 R^2, \end{cases} \quad v_s' = \begin{cases} \alpha s \left(\dfrac{R^2}{10} - \dfrac{r^2 + 2z^2}{14}\right) \\ -\beta s \left(\dfrac{R_0}{r}\right)^7 (r^2 - 5z^2), \end{cases} \quad v_z' = \begin{cases} -\alpha z \left(\dfrac{R^2}{5} - \dfrac{r^2 + s^2}{7}\right), & r \le R_0 \\ \beta z \left(\dfrac{R_0}{r}\right)^7 (2r^2 - 5s^2). & r > R_0 \end{cases} \tag{17a, b, c}$$

2.5. *Deformation of the Vortex-Ring Boundary*

The final adjusted solution (17a, b, c) no longer satisfies the condition of $\psi = 0$ at $r = R_0$. It follows that the boundary, R, of the vortex ring is no longer spherical, and a departure from this shape must be considered. To address this problem, we first recast the perturbation streamfunction into

$$\psi' = \begin{cases} \dfrac{s^2 z}{14} \left(\gamma R_0^2 - \alpha r^2\right), & r \le R, \\ -\beta s^2 z \dfrac{R_0^7}{r^5}, & r > R \end{cases} \tag{18}$$

by introducing an additional parameter, γ, so that there is more freedom to define the boundary, R, consistently. It also follows that

$$v_s' = \begin{cases} \dfrac{\alpha s}{14}(\tilde{\gamma} R_0^2 - r^2 - 2z^2) \\ -\beta s (\dfrac{R_0}{r})^7 (r^2 - 5z^2), \end{cases} \quad v_z' = \begin{cases} -\dfrac{\alpha z}{7}(\tilde{\gamma} R_0^2 - r^2 - s^2), & r \le R \\ \beta z (\dfrac{R_0}{r})^7 (2r^2 - 5s^2), & r > R, \end{cases} \tag{19a, b}$$

where $\tilde{\gamma} = \gamma/\alpha$.

The basic requirement to define the vortex-ring boundary is to seek a solution that satisfies

$$\psi\Big|_{r=R_-} = \psi\Big|_{r=R_+} = 0, \tag{20}$$

where $\psi = \bar{\psi} + \psi'$, and the subscripts $-$ and $+$ indicate the values from the internal and external solutions, setting an arbitrary constant for the streamfunction to be zero.

By substituting the general solution forms above, we obtain for $r \le R$,

$$\frac{\hat{\alpha}}{7\tilde{A}} \mu \tilde{R} (\tilde{\alpha} \tilde{R}^2 - \tilde{\gamma}) + \tilde{R}^2 - 1 = 0, \tag{21a}$$

and for $r > R$,

$$(\tilde{R}^3 - 1)\tilde{R} - 15\hat{\alpha}\tilde{\beta}\mu = 0. \tag{21b}$$

Here, we set $\mu = \cos\theta$, and

$$\tilde{R} = R/R_0, \tag{22a}$$

$$\hat{\alpha} = \alpha R_0/Q_0, \tag{22b}$$

$$\tilde{A} = A/Q_0 = -1/5, \tag{22c}$$

$$\tilde{\gamma} = \gamma/\alpha, \tag{22d}$$

$$\tilde{\beta} = \beta/\alpha. \tag{22e}$$

The fact that Eqs. (21a,b) are not identical leads to a difficulty in determining the vortex-ring shape consistently to higher orders under the present form of the solution, as seen immediately below.

Based on the form of the equations (21a,b), we seek a solution by the Taylor expansion

$$\tilde{R} = 1 + \sum_{n=1}^{N} \tilde{R}_n \mu^n, \tag{23}$$

with the truncation at N. After substituting this expression (23) into Eqs. (21a, b), the problem can be solved with increasing orders in powers of μ, by defining expansion coefficients, $\tilde{R}_n$. The results for $n = 1, 2, 3$ from the conditions (21a) and (21b), respectively, are:

$$\tilde{R}_1 = \frac{\hat{\alpha}}{14\tilde{A}}(\tilde{\gamma} - 1), \tag{24a}$$

$$\tilde{R}_2 = -\frac{\tilde{R}_1^2}{2} + \frac{\hat{\alpha}}{14\tilde{A}}(\tilde{\gamma} - 3)\tilde{R}_1 \tag{24b}$$

$$\tilde{R}_3 = -\tilde{R}_1\tilde{R}_2 + \frac{\hat{\alpha}}{14\tilde{A}}(\tilde{\gamma} - 3)\tilde{R}_2 - \frac{3}{14\tilde{A}}\hat{\alpha}\tilde{R}_1^2, \tag{24c}$$

and

$$\tilde{R}_1 = 5\hat{\alpha}\tilde{\beta}, \tag{25a}$$

$$\tilde{R}_2 = -2\tilde{R}_1^2, \tag{25b}$$

$$\tilde{R}_3 = \frac{20}{3}\tilde{R}_1^3. \tag{25c}$$

Here, the boundary deformation defined in terms of $\tilde{R}_n$ $(n = 1, 2, 3)$ above both from the internal and external solutions must be identical. Thus, for example, by comparing Eqs. (24a) and (25a), we find that the condition,

$$\frac{\tilde{\gamma} - 1}{14\tilde{A}} = 5\tilde{\beta},$$

must be satisfied. Also taking into account the consistency between Eqs. (24b) and (25b), we define the parameters as:

$$\tilde{\beta} = -\frac{2}{35}, \tag{26a}$$

$$\tilde{\gamma} = \frac{9}{5}. \tag{26b}$$

As a result, the boundary deformation is determined up to $n = 2$ in Eq. (23) consistently.

The obtained deformation tendency here is consistent with known numerical results (MJY, Lai *et al.* 2015, Tarshish *et al.* 2018, Leoanet and Jeevanjee 2019): Eqs. (25a) and (26a) show

that the vortex ring is displaced downwards at $O(\mu)$, and Eq. (25b) that the vortex ring is elongated in the lateral direction to $O(\mu^2)$.

However, by substituing these results into Eq. (24c), we find

$$\tilde{R}_3 = \frac{5}{4}\tilde{R}_1^3, \tag{27}$$

which is not consistent with Eq. (25c), thus the boundary deformation has been determined only up to $O(\mu^2)$ with the truncation $N = 2$. Above this order, the internal and external solutions cannot match properly.

2.6. *Presentation of the Solution*

In spite of its incompleteness, it is still worthwhile to examine the spatial structure of the steadily-propagating solution just derived, because it reproduces qualitatively well recent numerical results (MJY, Lai *et al.* 2015, Tarshish *et al.* 2018, Leoanet and Jeevanjee 2019) with an enhanced circulation to an upper half and a vertically squeezed vortex-ring shape, as shown by the bottom frame in Fig. 1.

Furthermore, thanks to the analytical procedure adopted, it is also possible to understand how this structure is generated: the leading-order solution (Hill's vortex: top frame) is modified in such a manner that the total potential vorticity, Q (Eq. 7b), is homogeneous inside the vortex ring ($r \leq R$) by compensating the background potential vorticity, αz, due to the buoyancy, increasing vertically, by a perturbation, ψ'. Thus, negative and positive vorticity perturbations must be generated, in compensation, to the upper and lower halves of the ring. That leads to a quadratic vorticity field in vertical section, as seen in the middle frame. As a result, a closed streamline defining the boundary of the vortex ring is squeezed downwards to maintain the continuity. This squeezing further leads to an enhancement of the circulation at the upper half as seen in the bottom frame. Note that the perturbation field itself tends to decrease and enhance the circulations, respectively, in the upper and the lower halves.

3. Unsteady Problem

Up to now, we have sought a steadily-propagating solution for a thermal vortex ring as a generalisation of Hill's vortex. However, such a solution should not exist in a strict sense, because the system (*cf.*, Eq. 6) is associated with a positive buoyancy averaged over the vortex-ring volume ($r \leq R$). Thus, the system must evolve in a unsteady manner by following a given buoyancy acceleration. This reflects upon the fact that the deformation of its boundary could be determined consistently only to the second order of a power series in $\mu = \cos\theta$ in Eq. (23). We may also note that the obtained steadily-propagating solution above also remains discontinuous in the tangential velocity along the vortex-ring boundary. This discontinuity will also be partially corrected in the following unsteady formulation (*cf.*, Eq. 36c).

Here, the "buoyancy acceleration" does not happen directly in the vertical direction. As an analysis of the impulse dynamics by Turner (1957) suggests, and as confirmed by Yano (2023), a differential buoyancy force acts on the vorticity (Eq. 1a) to expand the thermal with time. This expansion is often described by "entrainment" in the literature.

However, a representation of the dynamics of thermal vortex rings in terms of the entrainment rate is inherently limited in the sense that it cannot define their shapes. In the following, we are going to demonstrate that the expansion of the thermal vortex ring with time can be explained without explicitly introducing the entrainment in the formulation. This is a major difference from the dynamics of the entrainment plumes: the latter cannot be described properly without entrainment. Note that a thermal vortex ring will expand with time due to

its own vortex dynamics: no smaller–scale eddies are involved as the case with the entraining plume (*cf.*, Morton *et al.* 1956). Here, the buoyancy is advected outwards directly by the vortex–ring circulation, rather than by small–scale mixing; only the latter type of mixing can legitimately called the entrainment.

However, the whole picture is slightly more involved than just remarked. More precisely, the expansion is associated with outward spiral movements of fluid particles. In this respect, the boundary of the vortex ring becomes no longer a simple material surface in the same sense as for the entraining plume: a compensating advective inflow is required to conserve the total mass of the vortex ring, from a bottom along the ring axis. Because the inflow has no buoyancy, the overall spiral movement leads to a complex spiral structure of the buoyancy field.

Under these considerations, in this section, we generalise the formulation for the steadily-propagating vortex ring of previous sections to an unsteady problem. For this purpose, the axisymmetry assumption is maintained, and the time dependence is introduced by the separation of variables. Under these assumptions, those fine details just described cannot be properly represented, being effectively filtered out. As a result, the expansion of the thermal vortex ring is treated as a type of wave propagation, rather than that of a material surface. This last interpretation reflects the fact that the separation of variables implicitly introduces a homogenisation process. The attempt of this section is tentative at the best also due to the various additional approximations introduced in the analysis, and far from fully describing an expected complex structure just outlined. An important goal here is, nevertheless, to point out a possibility of constructing a self-contained analytical solution even for an unsteady state, and also consequently, to provide simple interpretations.

We first introduce, in the next subsection, the separation of variables, and solve the time dependence of the system. As it turns out, the remaining spatial dependency is analogous to the original steadily-propagating problem (Eqs. 7a and 5b), but adding inhomogeneous terms to the right-hand sides. Thus, we focus on deriving an inhomogeneous solution, to be designated as $\tilde{\psi}'$ for the streamfunction, for example. The inhomogeneous solutions is to be added to the original steadily-propagating solution, $\bar{\psi} + \psi'$, Thus, the full solution becomes:

$$\psi = \bar{\psi} + \psi' + \tilde{\psi}'. \tag{28}$$

We seek an inhomogeneous solution satisfying continuity of the streamfunction, buoyancy, as well as the tangential velocity at the vortex-ring boundary. The formulation of the problem presented in the following is general in the sense that by proceeding to the higher orders of the adopted Taylor expansions, the solutions can be derived to any desired orders.

In this study, however, to facilitate the analytical progress, the problem is solved under *linearisation* in respect to $\tilde{\psi}'$, by heavily truncating the Taylor expansions, but to an extent that it provides an enough freedom to satisfy the boundary conditions for the streamfunction and the buoyancy up to $O(\mu^3)$ under an expansion of the form (23). On the other hand, the continuity of the tangential velocity can be satisfied only up to $O(\mu)$ due to a technical reason. As a major departure from the steadily-propagating problem, the ordering by μ no longer follows that of $\hat{\alpha}$ under the unsteady problem. Here, a solution consistent to $O(\hat{\alpha})$ is sought, thus this truncation is also adopted in presenting the results subsequently. The following derivation is rather lengthy, and the technical details are provided separately in the Appendix.

Note that a basic analysis with the separation of variables of the same system has already been presented by Yano (2023). However, this study presents a new, closed-form analytical solution.

3.1. *Separation of Variables and Time-Dependence*

In order to take into account the unsteady evolution of the thermal vortex ring following Yano (2023), we introduce a time dependence by assuming the separation of variables to the potential vorticity, $q = \zeta/s$ and the buoyancy, b:

$$q = \hat{q}(t)\tilde{q}(\mathbf{r}/R_0), \tag{29a}$$

$$b = \hat{b}(t)\tilde{b}(\mathbf{r}/R_0) \tag{29b}$$

with $R_0 = R_0(t)$ now a time-dependent ring size, representing the expansion of the thermal with time. We also set $\psi = \hat{\psi}(t)\tilde{\psi}(\mathbf{r}/R_0)$ and $\mathbf{v} = \hat{\psi}(t)\tilde{\mathbf{v}}(\mathbf{r}/R_0)$. Note that Eqs. (29a, b) are a particular form of separable solutions, but being consistent with the form expected from the similarity solution suggested by Turner (1957) and Scorer (1957). We do not exclude a possibility of another solution form. However, such a solution is likely not be to in a closed form.

We further introduce re-scaled coordinates by

$$\xi = s/R_0, \quad \eta = z/R_0 \tag{29c}$$

so that the time derivative in equations becomes

$$\frac{\partial}{\partial t}\Big|_r = \frac{\partial}{\partial t}\Big|_\rho - \frac{\dot{R}_0}{R_0}\rho\frac{\partial}{\partial \rho}, \tag{29d}$$

where $\rho = r/R_0$, and the subscripts to the partial derivatives suggest a variable kept constant in operations. Note that the shape of the vortex ring, characterised by an angle-dependent radius, $R(\theta)$, evolves as the reference radius, $R_0(t)$, evolves with time by following the relation (22a). Furthermore, a perturbation buoyancy, b', must be added to the relation (6):

$$b = -\alpha\psi + b'. \tag{29e}$$

We also set: $b' = \hat{b}(t)\tilde{b}'(\mathbf{r}/R_0)$.

By substituting Eqs. (29a, b, c, d, e) into Eqs. (1a, b), we seek a consistent separable solution. Note first that the total buoyancy, $\bar{b}R_0^3$, is conserved in this system with $\bar{b}$ a vortex-ring volume averaged buoyancy, which suggests setting

$$\hat{b} = b_0/R_0^3(t) \tag{30a}$$

with b_0 a constant. As a result, the time dependence of the buoyancy is completely described in terms of the change in the vortex-ring radius, $R_0(t)$.

Realise further that to accomplish a separation of variables, all the other time dependency of the variables must also be described in terms of that of $R_0(t)$. As a result, Yano (2023) identifies the following forms

$$\hat{q} = \zeta_0/R_0^3(t), \quad \hat{\psi} = \zeta_0 R_0(t), \quad \alpha = \frac{\zeta_0}{R_0^4(t)}\hat{\alpha} \tag{30b, c, d}$$

with ζ_0 and $\hat{\alpha}$ constants. As also shown in Yano (2023), these conditions reduce the problem of time-dependence of the system into

$$R_0\dot{R}_0 = f\zeta_0 \tag{31a}$$

with a separation constant defined by $f(>0)$, which measures the buoyancy force acting on the expansion of the vortex ring. This leads to the known similarity solution (Scorer 1957) for the radius,

$$R_0(t) = (2f\zeta_0)^{1/2}t^{1/2} \tag{31b}$$

in an explicit manner. It also follows that the buoyancy and the potential-vorticity intensities also evolve as

$$\hat{b} \sim R_0^{-3} \sim t^{-3/2}, \quad \hat{q} \sim R_0^{-3} \sim t^{-3/2}.$$

A constant for the potential vorticity inside the vortex-ring core can also be set $Q_0 = \hat{Q}_0 \tilde{Q}_0$. Here, we have the freedom of partitioning a single constant into two constants. We find it convenient to introduce a normalisation $\tilde{Q}_0 = 1$. Thus, $\hat{Q}_0 = Q_0$, and it follows that

$$\zeta_0 = Q_0 R_0^3, \quad b_0 = Q_0^2 R_0^6. \tag{31c, d}$$

Finally, from the definition (14) of the phase speed, c, we find that c decreases with time by following an expansion of the thermal vortex rings as:

$$c = \frac{2Q_0 R_0^2}{15} = \frac{2}{15}\frac{\zeta_0}{R_0} \sim t^{-1/2}.$$

Here, the second equality is obtained with the help of Eq. (31c); the final result is obtained by further substituting the result (31b).

3.2. *Spatial Dependence of the System*

We are now left with the problem of solving the spatial dependence of the system, the problem left unaddressed by Yano (2023). This problem turns out to be a relatively straightforward extension of the steady propagation problem, with the original dependent variables replaced by the tilde variables, $\tilde{q}$, $\tilde{\psi}$, etc. By focusing on the spatial dependencies, the time dependencies designated by hats, $\hat{q}$, $\hat{\psi}$, etc. can simply be treated as normalisation factors for the variables, with the tilde variables as normalised counterparts.

As a result of the separation of the variables, the equations for the spatial dependencies are:

$$\tilde{J}(\tilde{Q}, \tilde{\psi}) = \xi f \left(3 + \rho \frac{\partial}{\partial \rho}\right) \tilde{q} - \frac{\partial \tilde{b}'}{\partial \xi}, \tag{32a}$$

$$\tilde{J}(\tilde{b}, \tilde{\psi}) = \xi f \left(3 + \rho \frac{\partial}{\partial \rho}\right) \tilde{b} \tag{32b}$$

in place of Eqs. (7a) and (5b). Here, all the notations are equivalent to those in Eqs. (7a) and (5b), but with the tilde added to suggest normalisations.

Note that apart from the normalisations, the left-hand sides of Eqs. (32a, b) are equivalent to those in the original equations, whereas the right-hand sides represent modifications due to the unsteadiness. In this respect, it is useful to designate the original steadily-propagating solutions (*i.e.*, homogeneous solutions) by the subscript h, and set:

$$\tilde{Q} = \tilde{Q}_h + \tilde{q}', \tag{33a}$$

$$\tilde{\psi} = \tilde{\psi}_h + \tilde{\psi}'. \tag{33b}$$

Here, we can set $\tilde{\psi}_h = \bar{\psi} + \psi'$, and their substitution into Eq. (7b) leads to an explicit definition of $\tilde{Q}_h$; $\bar{\psi}$ and ψ' are defined by Eqs. (13a) and (18), but resetting the constants to the normalised values, *i.e.*, $\tilde{A} = -1/5$ and $\tilde{c} \equiv c/Q_0 R_0^2 = 2/15$. The right-hand sides of Eqs. (32a, b) are found only in the interior of the vortex ring, $r \leq R$, thus only the modification to the interior solution due to the unsteadiness needs to be considered in the following.

Substituting Eqs. (33a, b) into Eqs. (32a, b), and after linearisation in respect to $\tilde{\psi}'$, ne-

glecting the terms, $\tilde{J}(\tilde{q}', \tilde{\psi}')$ and $\tilde{J}(\tilde{b}', \tilde{\psi}')$, in both equations, we obtain

$$\tilde{J}(\tilde{q}', \tilde{\psi}_h) = \xi f(3 + \rho\frac{\partial}{\partial\rho})\tilde{q} - \frac{\partial\tilde{b}'}{\partial\xi}, \tag{34a}$$

$$\tilde{J}(\tilde{b}', \tilde{\psi}_h) = \xi f(3 + \rho\frac{\partial}{\partial\rho})(-\hat{\alpha}\tilde{\psi} + \tilde{b}'), \tag{34b}$$

keeping in mind that $\tilde{q} = \tilde{q}_h + \tilde{q}'$ and $\tilde{\psi} = \tilde{\psi}_h + \tilde{\psi}'$ in the right-hand sides. Linearisation, adopted here for facilitating an analytical progress, should not have severe consequences, because only a modification of $O(\hat{\alpha})$ due to the unsteadiness is required to the original solution.

Eqs. (34a, b) can be solved by setting

$$\tilde{q}' = \sum_{n,m} q_{nm}\xi^n\eta^m, \tag{35a}$$

$$\tilde{\psi}' = \sum_{n,m} \psi_{nm}\xi^n\eta^m, \tag{35b}$$

$$\tilde{b}' = \sum_{n,m} b_{nm}\xi^n\eta^m, \tag{35c}$$

where q_{nm}, ψ_{nm}, and b_{nm} are the expansion coefficients. By substituting Eqs. (35a, b, c) into Eqs. (34a, b), we obtain recursion relations for q_{nm} and b_{nm}. By symmetry of the system, the odd coefficients, $\psi_{2n+1,m}$, vanish. As already remarked, these Taylor series can solve this linearised problem up to any orders of accuracy by proceeding to the higher-order terms. However, for now, with the goal of solving the problem accurately up to $O(\mu^3)$, the expansion is terminated at $n = 3$ and $m = 3$ for $\psi_{2n,m}$.

3.3. *Boundary Conditions*

The following three conditions are imposed at the vortex-ring boundary, $r = R$:

$$\psi = 0, \tag{36a}$$

$$b = 0, \tag{36b}$$

$$\mathbf{n}\cdot\nabla\left(\psi\Big|_{r=R+} - \psi\Big|_{r=R-}\right) = 0 \tag{36c}$$

with $\mathbf{n}$ a vector normal to the vortex-ring boundary, which is defined by:

$$\mathbf{n}\cdot\nabla = \sigma_s\frac{\partial}{\partial s} + \sigma_z\frac{\partial}{\partial z}, \tag{37}$$

where

$$\sigma_s = (1 + 2\tilde{R}_1\mu + 3\tilde{R}_2\mu^2 + 4\tilde{R}_3\mu^3)\sin\theta,$$

$$\sigma_z = -\tilde{R}_1 + (1 - 2\tilde{R}_2)\mu + (2\tilde{R}_1 - 3\tilde{R}_3)\mu^2 + 3(\tilde{R}_2 - \tilde{R}_3)\mu^3 + 4\tilde{R}_3\mu^4$$

recalling the definitions (22a) and (23). Also keep in mind that the external boundary conditions (25a, b, c) for the steadily-propagating solutions are still valid for the unsteady case here.

Note that the boundary condition on the buoyancy (36b) must be considered separately in the unsteady problem, because the unsteady correction, $\tilde{b}'$, to the buoyancy is determined separately from the streamfunction, no longer satisfying the relation (6). The last condition (36c) ensures the continuity of the velocity at the vortex-ring boundary. However, for the reason explained in the Appendix (*cf.*, Eqs. A.3a, b, c), application of this last boundary

condition must be terminated at $O(\mu)$ in expansion in μ. We believe that this additional constraint arises due to a limitation of assuming a similarity form of the solution (29a, b).

These three conditions reduce to

$$\frac{\tilde{A}}{2}(1-\tilde{R}^2)+\hat{\alpha}\frac{\tilde{\gamma}-\tilde{R}^2}{14}\mu\tilde{R}+\sum_{n=0}^{\infty}\lambda_n\mu^n=0, \tag{38a}$$

$$\frac{\hat{\alpha}\tilde{A}}{2}(1-\tilde{R}^2)+\frac{\hat{\alpha}^2\mu}{14}(\tilde{\gamma}-\tilde{R}^2)\tilde{R}=\sum_{n=0}^{\infty}B_n\mu^n, \tag{38b}$$

$$\sum_{n=0}^{3}[\sigma_s(\tilde{W}D_n+\hat{\alpha}E_n-2F_n)+\sigma_z(\tilde{W}G_n+\hat{\alpha}H_n-2K_n)]=0, \tag{38c}$$

where the coefficients, λ_n, σ_s, σ_z, B_n, D_n, E_n, F_n, G_n, H_n, and K_n are defined in the Appendix.

These three boundary conditions are solved in the increasing order of μ up to $O(\mu^3)$ for (38a, b) and $O(\mu)$ for (38c). It leads to the 10 conditions, with the leading order $O(\mu^0)$, to be satisfied with the parameters, $\tilde{\beta}$, $\tilde{\gamma}$, and $\tilde{f}=f/\hat{\alpha}$, and the coefficients, q_{20}, b_{20}, b_{40}, ψ_{20}, ψ_{21}, ψ_{22}, ψ_{23} to be determined. Here, note the nonlinearity in the boundary conditions (38a, b), thus the obtained solutions are not superposable, although the governing equation (34a, b) has been linearised.

To avoid analytical complexities, these coefficients are defined only to the leading orders with all the contributions above $O(\hat{\alpha})$ neglected: this is not as major compromise as it may appear because we can still define the vortex-ring form to a higher order in μ than it was possible with a purely-propagating assumption in the last section.

After a lengthy deduction outlined in the Appendix, the leading-order coefficients are determined to be:

$$\tilde{f}=\frac{448}{44785}+O(\hat{\alpha})\simeq 0.0100, \tag{39a}$$

$$\tilde{\psi}_{21}=-\frac{2402}{24115}+O(\hat{\alpha})\simeq -9.96\times10^{-2}, \tag{39b}$$

$$\tilde{\psi}_{23}=\frac{192}{4823}+O(\hat{\alpha})\simeq 0.0398, \tag{39c}$$

$$\tilde{\gamma}=14(\tilde{\gamma}_0-\tilde{\beta})+O(\hat{\alpha}), \tag{39d}$$

where $\tilde{\psi}_{21}=\hat{\alpha}^{-1}\psi_{21}$, $\tilde{\psi}_{23}=\hat{\alpha}^{-1}\psi_{23}$, and

$$\tilde{\gamma}_0=\frac{69873}{626990}+O(\hat{\alpha})\simeq 0.111.$$

Finally, the boundary-deformation parameter, $\tilde{\beta}$, is determined from the second-order polynomial equation:

$$\left(2-\frac{39}{4\tilde{A}}\tilde{f}\right)\tilde{\beta}^2+\left[\frac{1}{2}\left(\frac{13}{14}-\tilde{\gamma}_0\right)+13\tilde{f}\right]\tilde{\beta}+\frac{3}{2}\tilde{f}\left[\frac{1}{14}-7\tilde{\gamma}_0+(19+\frac{1}{\tilde{A}})\tilde{f}\right]-3\tilde{f}\left(3\tilde{\psi}_{21}-\tilde{\psi}_{23}\right)=0. \tag{39e}$$

The other coefficients turn to be $O(\hat{\alpha}^2)$, and are neglected in the following presentations.

By solving Eq. (39e), we obtain two eigenvalues for $\tilde{\beta}$: a large positive value (0.213) and a slightly negative value (-3.07×10^{-3}). These two eigenvalues lead to the two nonlinear eigensolutions, which are referred as the first and the second modes, respectively. The basic parameters of those two eigensolutions are listed in Table 1 along with those for the steady-propagation derived in the last section. Keep in mind that the nondimensional buoyancy parameter, $\tilde{\alpha}$, remains a free parameter of the problem even for the unsteady case.

Table 1. Basic Parameters of the Obtained Modes

	$\tilde{\beta}$	$\tilde{\gamma}$
Steadily-propagating solution	-5.71×10^{-2}	1.8
First Mode	0.213	4.55
Second Mode	-3.07×10^{-3}	1.60

The streamfunctions in Figs. 1 and 2 are obtained with the above parameters from a general formula (28) with $\bar{\psi}$ and ψ' defined by Eqs. (13a) and (18), respectively. For the steadily-propagating solution, $\tilde{\psi}' = 0$, and for the unsteady solutions, $\tilde{\psi}'$ is defined by Eq. (35b) with the leading coefficients defined by Eqs. (39b, c), and higher coefficients determined by the recursion relation (A.1c).

The obtained solution for the first mode shown in Fig. 2(a), with $\hat{\alpha} = 0.3$, compares well with that of MJY (see their Fig. 6). A top heavy circulation of the thermal vortex ring is also found in Lai *et al.* (2015, Fig. 7) as well as a composite by Romps and Chrain (2015, Fig. 10). However, the composite of the latter work presents a vertical elongation of the vortex ring. On the other hand, the tendency of the thermal vortex ring to elongate horizontally is also identified by Tarshish *et al.* (2018, their Fig. 3), and Leoanet and Jeevanjee (2019, their Fig. 2).

The second mode leads only to a very weak deformation of the boundary, which is hardly visible graphically (Fig. 2(b)) even when $\hat{\alpha}$ is set fairly large ($\hat{\alpha} = 1$ here). The continuity of the solution is, instead, accomplished by more explicitly adding and subtracting the vorticity at the top and the bottom of the vortex ring, as seen in the middle frame. As a result, a top heavy circulation also appears.

4. Comparisons with Numerical Results

Two nonlinear eigensolutions have been obtained analytically for a given buoyancy parameter, $\hat{\alpha}$, in the last section. As an application, we principally perform the analysis of the momentum budget of those obtained solutions in this section. The purpose here is the two-fold: to test whether the obtained analytical solutions can reproduce the numerical results with higher resolutions, notably by Morrison *et al.* (2022, MJY). The analytical result here can, in turn, provide a physical interpretation for those numerical results. Keep in mind that all the following results are based on truncation at $O(\hat{\alpha})$.

4.1. *Geometrical Factor*

Before proceeding to the momentum budget, we briefly examine the geometrical factor, Γ, which is defined by

$$\Gamma = \pi R_0^3 / V, \tag{40}$$

because it is the best quantity to characterize the evaluated deformation of the vortex-ring shape. Here, V is the volume of the vortex ring, which is evaluated by:

$$V = 2\pi \int_0^{\pi} \int_0^{R(\theta)} r^2 \sin\theta dr d\theta = \frac{2\pi}{3} \int_0^{\pi} R^3(\theta) \sin\theta d\theta = \frac{2\pi}{3} R_0^3 \int_{-1}^{1} \tilde{R}^3(\mu) d\mu. \tag{41}$$

In this evaluation, we only consider the terms up to $O(\mu^3)$ in $\tilde{R}^3$:

$$\tilde{R}^3 \simeq 1 + 3\tilde{R}_1\mu + 3(\tilde{R}_1^2 + \tilde{R}_2)\mu^2 + (\tilde{R}_1^3 + 3\tilde{R}_3 + 6\tilde{R}_1\tilde{R}_2)\mu^3.$$

This truncation rule to $O(\mu^3)$ will be applied systematically to any expressions, $\tilde{R}^n$, with an integer, n, without remark in the following.

The final result is:

$$V = \frac{4}{3}\pi R_0^3 \tilde{V}, \tag{42a}$$

where

$$\tilde{V} \simeq 1 - \tilde{R}_1^2. \tag{42b}$$

By substituting the expression (42a) into Eq. (40), the latter reduces to:

$$\Gamma = \frac{3}{4\tilde{V}}. \tag{43}$$

Because the vortex-ring shape of the first mode is vertically squeezed with the increasing buoyancy effect, $\hat{\alpha}$, the normalised volume decreases with the increasing $\hat{\alpha}$, thus the geometrical factor (40) increases with the increasing $\hat{\alpha}$, as shown by the solid curve in Fig. 3. MJY shows $\Gamma \simeq 1$ in their similarity regime. We find from the plot that this value is obtained with $\hat{\alpha} \simeq 0.5$ with the first mode. On the other hand, the geometrical factor of the second mode (long dash) remains almost perfectly that of the sphere, $\Gamma = 3/4$, for the full range of $\hat{\alpha}$ on plot.

4.2. *Momentum Budget: Formulation*

The momentum equation to be considered is:

$$\frac{dw}{dt} = -\frac{1}{\rho}\frac{\partial p_d}{\partial z} - \frac{1}{\rho}\frac{\partial p_b}{\partial z} + b. \tag{44}$$

Here, the pressure, p, has been decomposed into the dynamic and the buoyancy contributions by setting, $p = p_d + p_b$.

After a volume average, we obtain a standard description for the momentum budget of a vortex ring (*cf.*, Morrison *et al.* 2022):

$$\frac{d\langle w\rangle}{dt} = -\frac{1}{\rho}\langle\frac{\partial p_d}{\partial z}\rangle - \frac{1}{\rho}\langle\frac{\partial p_b}{\partial z}\rangle + \langle b\rangle + E. \tag{45}$$

Here, the bracket, $\langle * \rangle$, indicates the average over the vortex-ring volume, and the last term, E, represents a contribution of the change of the vortex-ring volume with time, commonly called "entrainment". In the following diagnosis, the volume-averaged vertical velocity is set equal to the propagation speed, *i.e.*, $\langle w\rangle = c$, as expected for a quasi-steadily propagating solution.

4.3. *Pressure Problem*

Recall that the dynamic and buoyancy pressures, p_d and p_b, are obtained by solving the Poisson problems:

$$\frac{1}{\rho}\nabla^2 p_d = -\nabla\cdot(\mathbf{v}\cdot\nabla\mathbf{v}), \tag{46a}$$

$$\frac{1}{\rho}\nabla^2 p_b = \frac{\partial b}{\partial z}. \tag{46b}$$

Here, by considering the solution only to $O(\hat{\alpha})$, the source terms on the right-hand sides are also truncated at $O(\hat{\alpha})$. For this reason, the buoyancy is more specifically approximated by

$b \simeq -\hat{\alpha}\psi$ with $\psi \simeq \bar{\psi}$. The contribution of $\tilde{b}'$ is found only at $O(\hat{\alpha}^2)$. Eqs. (46a,b) are solved by expanding both p_d and p_b with the Legendre functions, $P_n(\mu)$, thus

$$p = \sum_{n=1}^{N} \tilde{p}_n(r) P_n(\mu) \tag{47}$$

with the subscripts d and b are to be added for the two pressure components.

The problem is solved by posing the continuity of the pressure up to the first derivative at the vortex-ring boundary, $r = R(\theta)$, in the normal direction, where the normal direction, $\mathbf{n}$, is defined by Eq. (37). Here, also for solving this boundary problem with facility, we apply the Taylor expansion to these boundary conditions under in terms of $R - R_0$ up to the first order, *i.e.*,

$$\Delta p\Big|_{r=R} \simeq \Delta p\Big|_{r=R_0} + \frac{\partial \Delta p}{\partial r}\Big|_{r=R_0}(R - R_0)$$

$$\frac{\partial \Delta p}{\partial r}\Big|_{r=R} \simeq \frac{\partial \Delta p}{\partial r}\Big|_{r=R_0} + \frac{\partial^2 \Delta p}{\partial r^2}\Big|_{r=R_0}(R - R_0),$$

consistent with the general strategy of truncation at $O(\hat{\alpha})$. Here, Δp is the difference of the external and internal pressure solutions. The expansion in Legendre functions is truncated at $N = 6$: this rather strong truncation is adopted by considering the degree of truncation in the unsteady solution given by Eqs. (35a, b, c).

The obtained pressures, p_d and p_b, will be presented in terms of the volume average. This last step is facilitated by noting that the pressure gradient averaged over the vortex-ring volume is given, after a partial integral, by:

$$V\left\langle \frac{\partial}{\partial z}\left[\frac{p}{\rho}\right]\right\rangle = 2\pi \int_0^{R(\theta=\pi/2)} \left[\frac{p}{\rho}\right]_{-R(-\mu)\mu}^{z=R(\mu)\mu} sds$$

$$= 2\pi R_0^2 \int_{-1}^{1} \left[\frac{p}{\rho}\right]_{r=R} \Lambda(\mu) d\mu, \tag{48a}$$

where

$$\Lambda(\mu) = \tilde{R}^2\mu - \tilde{R}\frac{d\tilde{R}}{d\mu}(1-\mu^2). \tag{48b}$$

Its explicit form is obtained by substituting Eq. (23) with $N = 1$, corresponding to the truncation at $O(\hat{\alpha})$.

The dynamic pressure acting on the thermal vortex ring is often represented as a drag force in terms of a drag coefficient, C_d, as:

$$\frac{1}{\rho}\langle\frac{\partial p_d}{\partial z}\rangle = \frac{\Gamma}{2} C_d \frac{c^2}{R_0}, \tag{49}$$

where Γ is the geometrical factor defined by Eq. (43). In turn, the buoyancy pressure can be considered a force counteracting against the buoyancy; thus the effective buoyancy, b_e, may be defined by

$$b_e = -\frac{1}{\rho}\langle\frac{\partial p_b}{\partial z}\rangle + \langle b\rangle. \tag{50a}$$

It may alternatively be expressed as

$$b_e = C_v\langle b\rangle \tag{50b}$$

in terms of the virtual mass coefficient, C_v (*cf.*, de Roode *et al.* 2012, Tarshish *et al.* 2018). Note that some works alternatively define the virtual mass coefficient, γ_v, by setting $C_v = (1+\gamma_v)^{-1}$

(*e.g.*, Simpson and Wiggert, 1969, Haman and Malinowski 1989, Bechtold *et al.* 2001).

4.4. *Pressure gradient at infinity*

.

As going to be seen in the next two subsections, the results with the pressure-gradient forces tend to be rather singular. Inspection of both dynamic and buoyancy pressure fields suggests that this is due to strong distortions of the pressure fields around the vortex-ring boundary.

As seen in Sec. 2, singularities arise along the boundary in attempt of constructing a steadily-propagating thermal vortex ring solution: first, the vortex-ring boundary cannot be determined consistently in such a manner that boundary corresponds to a constant streamfunction line. Moreover, the attempted construction of the solution still leaves further discontinuities in the velocity and the buoyancy: the tangent component of the velocity remains discontinuous along the boundary leading to infinite shear. The buoyancy also remains discontinuous, leading to discontinuity of the buoyancy-gradient force crossing the vortex-ring boundary.

All those discontinuities have been designed to be removed in constructing the unsteady solution in the last section. However, the obtained solution still retains steep gradients close to the boundary due to a severe truncation adopted in constructing the solutions. The strong steepness around the boundary further leads to abnormal behaviours in pressure gradients.

A possible way of avoiding those singular tendencies is to move the boundary for evaluating the average pressure gradients to infinity: averaging it over a sphere of the radius, r, and taking the asymptotic limit, $r \to \infty$. Thus, the average pressure gradient is evaluated as:

$$\langle \frac{\partial p}{\partial z} \rangle = \frac{4\pi r^3/3}{V} \langle \frac{\partial p}{\partial z} \rangle \Big|_{r\to\infty}, \tag{51}$$

where $\langle \partial p/\partial z \rangle|_{r\to\infty}$ indicates the average is computed in the limit, $r \to \infty$ over a sphere with a radius r. Substituting (47) into Eq. (51) we find:

$$\langle \frac{\partial p}{\partial z} \rangle = \frac{4\Gamma}{3} \hat{p}_1 \tag{52}$$

to the leading order, noting that $\tilde{p}_1(r) = \hat{p}_1 r^{-2}$ for the external pressure with $\hat{p}_1$ a constant, both for the dynamic and buoyancy pressures. This formula (52) permits us to evaluate the pressure gradients in terms only of a single expansion coefficient, $\hat{p}_1$.

4.5. *Dynamic-Pressure Drag*

The drag coefficients, C_d, evaluated for the two nonlinear modes obtained in the last section are plotted in Fig. 4 as functions of $\hat{\alpha}$. These results can be qualitatively interpreted by invoking the Bernoulli principle obtained for the dynamic pressure:

$$\frac{p_d}{\rho} = -\frac{\mathbf{v}^2}{2} + \text{const.} \tag{53}$$

especially for the steadily-propagating component of the solution, although the principle does not strictly apply to the unsteady component. Since the vortex-ring circulation is squeezed upwards with both modes, it is expected that the circulation is also overall enhanced in the upper side of the vortex ring. With a simple application of the Bernoulli principle (53), it follows that the dynamic pressure force must overall act positive upwards, being associated with a negative pressure drag.

The results in Fig. 4 based on Eqs. (48a, b) present a rather excessively negative C_d for both modes (solid and long dash), with an overall monotonically decreasing tendency with $\hat{\alpha}$, except for a singular behaviour found with the first mode (solid) at $\hat{\alpha} \simeq 0.4$, and also a

bounce back above $\hat{\alpha} \simeq 0.8$. The dynamic-pressure drag for first mode (short dash) evaluated at infinity by Eq. (52) more consistently decreases with the increasing $\hat{\alpha}$. After removing the singular behaviour of the dynamic pressure field around the boundary, the drag, C_d, becomes even more excessively negative. the average over the vortex-ring volume (*cf.*, Eqs. 48a, b: short dash). On the other hand, the curve for the second mode with Eq. (52) perfectly matches that with the average over the vortex-ring volume (*cf.*, Eqs. 48a, b: long dash).

The negative drag coefficient, C_d, obtained here is qualitatively consistent with the result of MJY. However, estimated values herein are most likely exaggerated due to a strong truncation of the solution at $O(\hat{\alpha})$: MJY obtained only a modest negative value with $C_d \simeq -0.1$. As already remarked in the beginning of Sec. 4.4, these singularities found with the first mode are consequences of artificial "resonances" resulting from a strong truncation in Eq. (47), which cannot remove strong pressure gradients over the vortex-ring boundary.

4.6. *Buoyancy Pressure*

Fig. 5 shows the results for the virtual mass coefficient, C_v (*cf.*, Eq. 50b). For both modes (solid and long dash) obtained by the direct evaluation (48a, b) over the vortex volume, the reduction of the virtual mass, C_v, from the normalised value is rather small (just about 5%). The first mode (solid) even increases with the increasing $\hat{\alpha}$, and C_v surpasses unity at $\hat{\alpha} \simeq 0.35$.

The virtual mass, C_v, evaluated with the pressure gradient at infinity (Eq. 52), is more sensible with the first mode (short dash): it overall monotonically decreases with increasing $\hat{\alpha}$ by following from an expected tendency of the buoyancy pressure to counteract the buoyancy force, apart of singular oscillations due to a heavy truncation of the solution. The adopted asymptotic limit successfully removes a singular behaviour of the buoyancy pressure around the vortex-ring boundary. A high-resolution simulation result by MJY with $C_v \simeq 0.5$ is recovered at $\hat{\alpha} \simeq 0.35$. This value is not very far from an estimate, $\hat{\alpha} \simeq 0.5$, obtained by fitting the value of the geometrical factor, Γ, with MJY's result in Fig. 3.

On the other hand, the second mode simply presents a constant with $\hat{\alpha}$ on the plot both for the direct evaluation (48a, b: long dash) and the pressure at infinity (52: chain dash). The change of the evaluation method merely changes a constant value, with a smaller value for the latter. Thus, we conclude that the first nonlinear mode is more relevant than the second for interpreting the numerical results by MJY. Note that MJY's simulation is initiated with a homogeneous spherical buoyancy anomaly with a quiescent state. This particular initial condition leads to the first nonlinear mode.

5. Summary and Conclusions

An analytical solution of a thermal vortex ring has been derived from a consideration of the vortex dynamics. This system is described by a type of potential vorticity, $q = \zeta/s$, defined in terms of the azimuthal vorticity, ζ, and the distance, s, from the vertical axis of the vortex ring. This potential vorticity is conserved in the absence of buoyancy because a vortex ring can be considered a ring-shaped vortex tube, in which its circle plays a role of the length of a vortex tube.

When the buoyancy is added to this system, it acts on the potential vorticity as a differential force (*cf.*, Eq. 1a). Furthermore, under a steady-propagation assumption, this term can be interpreted in analogy with the β-effect of quasi-geostrophic flows, in which a "background vorticity" induced by buoyancy increases with height. When the buoyancy is assumed to be proportional to the local streamfunction, this analogue β-parameter becomes a constant, α, as assumed herein. Thus, in the presence of buoyancy, a total potential vorticity, $Q = q + \alpha z$,

including the background potential vorticity induced by buoyancy, is conserved under the steadily-propagation assumption.

Under this framework, the classical solution of Hill's vortex is obtained by assuming a constant potential vortitcy inside a sphere in the absence of buoyancy. Generalisation of this solution to the buoyant case is straightforward in the potential vorticity framework just outlined (*cf.*, Flierl 1987): the presence of the background vorticity induced by buoyancy adds "perturbation" terms to Hill's solution, which can also be solved in a fully nonlinear manner. The generated perturbation fields take a form of a quadratic vorticity in vertical section as expected from an analogy of the buoyancy effect with the β effect.

The difficulty in completing this solution is that the presence of buoyancy makes the vortex ring no longer perfectly spherical, as with Hill's vortex. It has been sought to determine the deformation of the vortex-ring boundary by assuming a form (23) of power series in $\mu = \cos\theta$, where θ is an angle away from the vortex-ring axis. However, as it turns out, it has been possible to determine the deformation only up to $O(\mu^2)$. Beyond this order, the internal and external solutions remain unmatched. However, importantly, this incomplete solution (Fig. 1) already depicts well the tendency of thermal vortex rings to flatten in vertical direction, as seen in numerical simulations (Morrison *et al.* 2022, Lai *et al.* 2015, Tarshish *et al.* 2018, Leoanet and Jeevanjee 2019).

Physically speaking, the difficulty of completing a steadily-propagation solution stems from the fact that a thermal vortex ring cannot be purely propagating vertically, but evolves unsteadily because there is always a net upward buoyancy force. The original steady formulation has been modified by accounting for the time-dependence by the separation of variables. This formulation reduces the time dependency into that of the radius of the vortex ring, which can be shown to evolve as $\sim t^{1/2}$, as expected from the similarity solution (Scorer 1957). The remaining problem of spatial dependence remains close to the original steadily-propagating problem except for additional inhomogeneous terms arising from the unsteadiness. Inclusion of these effects permit determining the deformation of the vortex-ring boundary to any arbitrary order of power series in $\mu = \cos\theta$ with the help of an infinite series of undetermined coefficients, $q_{2n,0}$ $(n = 1, \ldots)$, in Taylor expansion (35a). Here, the problem is solved to $O(\mu^3)$. The solution is determined accurately to $O(\hat{\alpha})$ accordingly, where $\hat{\alpha}$ is a normalised version of the β-parameter (or buoyancy parameter) of the problem, as defined by Eq. (22b). As a result, the streamfunction solution is modified at $O(\hat{\alpha})$ due to the unsteadiness, whereas the modification to the buoyancy remains to $O(\hat{\alpha}^2)$, thus not explicitly considered. Here, for facilitating the analytical solution, the inhomogeneous equation for the unsteady problem has been linearised in respect to an unsteady component of the variable. The unsteady component has been solved under Taylor expansions with a relatively severe truncations, as well.

The two nonlinear eigensolutions, with a nonlinearity arising from the boundary conditions (38a, b, c), are identified: both are characterised by stronger circulations to the vortex ring at the upper half. However, these two solutions achieve this configuration in qualitatively different manners. The first mode consists of a noticeable displacement of the vortex-ring boundary downwards. As a result, the vortex-ring circulation is squeezed in upper half (Fig. 2(a)). On the other hand, the second mode generates this structure by more directly adding and subtracting the vorticity at the upper and from the lower halves, respectively (Fig. 2(b)). In this case, the vortex ring hardly deforms from an original spherical shape. Note that in both cases, further modifications due to the unsteadiness tend to cancel out a quadratic structure generated by the buoyancy "β" effect inside the vortex ring ($r < R(\theta)$): under the unsteady regime, the buoyancy "β" effect (*or* baroclinic forcing) mostly works as a driving force for expanding the thermal vortex ring with time, in the analogous manner as the normal β-effect leads to Rossby waves.

An immediate consequence expected from a stronger circulation at the upper half is an upward dynamic pressure-gradient force, associated with a negative dynamic-pressure drag,

as inferred qualitatively from the Bernoulli principle (53). This result is also qualitatively consistent with a diagnosis from a high-resolution numerical simulation by Morrison *et al.* (2022, MJY). However, the negative drags obtained from the analytical solutions are most likely exaggerated due to the fact that only the leading terms have been considered in unsteady contributions. In contrast, only a weakly negative drag coefficient, $C_d \simeq -0.1$, is found in MJY's numerical simulation.

On the other hand, the virtual mass, C_v, based on the buoyancy-pressure gradient averaged over an asymptotically large sphere, as well as the geometrical factor, Γ, provide reasonable agreements with those obtained by MJY with the buoyancy parameter, $\hat{\alpha} \simeq 0.35$–0.5, for the first nonlinear eigensolution: this overall consistency of the estimated buoyancy parameter, $\hat{\alpha}$, is remarkable, considering various simplifications involved in the present study. In contrast, the deformation of the second solution is too weak to be compared with the numerical result by MJY.

Analytical solutions can elucidate physical aspects not immediately obvious from numerical simulations: a close equivalence of the present system with the quasi-geostrophy with an β effect played by the buoyancy parameter, α, is most notable. At the same time, some of the results are not quantitatively satisfactory, most notably, a highly exaggerated negative dynamics-pressure drag. The limitations of the obtained results are due to various simplifications introduced in this study. These are divided into two major categories: physical and mathematical. Physically speaking, the formulation is developed under the Boussinesq approximation, and with further simplifications. The most notable is a linear relationship between the buoyancy and the streamfunction inside the vortex-ring core assumed in the steadily-propagating solution. The separation of variables adopted in deriving the unsteady evolution of the vortex ring may also be pointed out. However, this last simplification is likely to be less severely restrictive than it appears, with the focus of this study on the similarity regime, in which the circulation pattern of the vortex ring is overall conserved with time associated with its expansion. Nevertheless, few subtle issues are expected, as already remarked at the beginning of Sec. 3.

The unsteady solutions have been derived under further mathematical simplifications. First, an inhomogeneous problem for the correction terms due to the unsteadiness is solved under the linearisation of those terms. The solutions have been further restricted by applying a severe truncation in the Taylor expansions. These simplifications have been necessary to facilitate the analytical progress, which would become much more tedious otherwise. They can certainly be relaxed, and the steps to be taken would be further facilitated by a more numerically-oriented approach, such as a spectral method proposed by Boyd and Ma (1990), for example.

Appendix: Solution Procedures

This appendix provides details of the derivation of the solution in Sec. 3.

A.1. Recursion Relations

The recursion relations to be solved for q_{nm} and b_{nm} are:

$$(m+1)\tilde{A}q_{n,m+1} + [(3+n+m)f - \frac{n-2m}{14}\gamma]q_{nm} + (n-m+1)\tilde{A}q_{n,m-1}$$
$$+\frac{3n-2m+4}{14}\hat{\alpha}q_{n,m-2} - 2(m+1)\tilde{A}q_{n-2,m+1} + \frac{n-4m-2}{14}\hat{\alpha}q_{n-2,m}$$
$$+ \delta_{n0}\delta_{m0}3f\tilde{Q}_0 - \delta_{n0}\delta_{m1}4\hat{\alpha}f = (n+2)b_{n+2,m}, \tag{A.1a}$$

$$(m+1)\tilde{A}b_{n,m+1} + [(3+n+m)f - \frac{n-2m}{14}\gamma]b_{nm} + (n-m+1)\tilde{A}b_{n,m-1} + \frac{3n-2m+4}{14}\hat{\alpha}b_{n,m-2}$$
$$- 2(m+1)\tilde{A}b_{n-2,m+1} + \frac{n-4m-2}{14}\hat{\alpha}b_{n-2,m} + F_{nm} = 0. \tag{A.1b}$$

Here, δ_{n0}, δ_{m0}, and δ_{m1} are Kronecker's delta, and $\tilde{Q}_0 = 1$ is retained above as a marker for the origin of the term, and.

$$F = -\hat{\alpha}f(3+\rho\frac{\partial}{\partial\rho})\tilde{\psi} \equiv \sum_{n,m} F_{nm}\xi^n\eta^m,$$

From Eq. (A.1a), the series, q_{0m} $(m = 1, 2, \ldots)$ is first obtained by setting $n = 0$ with $q_{00} = 0$, then we proceed incrementally to a higher n. At each n, the leading coefficient q_{n0} remains undetermined, but the subsequent coefficients, q_{nm} with $m > 0$ are determined in terms of the former. These leading coefficients, q_{n0}, provide freedom to satisfy the boundary condition (20) to any order in μ.

From the determined Taylor series of q, the streamfunction can be determined from Eq. (4c). Thus, its coefficients, $\{\psi_{nm}\}$ are obtained from $\{q_{nm}\}$ by a recursion relation,

$$\psi_{n+4,m} = \frac{-(m+2)(m+1)\psi_{n+2,m+2} + q_{nm}}{(n+4)(n+2)}, \tag{A.1c}$$

setting $\psi_{0m} = 0$. It follows that

$$\psi_{4,m} = \frac{q_{0m}}{8} - \frac{(m+2)(m+1)}{8}\psi_{2,m+2},$$
$$\psi_{6,m} = \frac{-(m+2)(m+1)\psi_{4,m+2} + q_{2m}}{24}$$

for $m = 0, 1, \ldots$.

The buoyancy coefficients, b_{nm}, are in turn, determined from Eq. (A.1b). Here, $F_{0m} = 0$ for all m, and we find $b_{0m} = 0$ $(m = 0, \ldots)$ from the boundary condition (36b). The procedure for $n \geq 2$ begins with $m = 1$ in the increasing order of m, with b_{n0} left to be determined from the boundary condition. Keep in mind that the resulting buoyancy correction, $\tilde{b}'$, due to the unsteadiness further influences the potential vorticity, $\tilde{q}'$, through the right-hand side of Eq. (A.1a).

A.2. Boundary Conditions

The condition (36a) at $r = R$ is immediately re-written as:

$$\bar{\psi} + \psi' + \tilde{\psi}' = 0,$$

which further reduces to (38a) with the parameters defined by

$$\lambda_0 = \psi_{20} + \psi_{40} + \psi_{60},$$
$$\lambda_1 = \psi_{21} + \psi_{41} + \psi_{61} + 2\tilde{R}_1(\psi_{40} + 2\psi_{60}),$$
$$\lambda_2 = \psi_{22} + \psi_{42} + \psi_{62} - \psi_{40} - 2\psi_{60} + \tilde{R}_1(\psi_{21} + 3\psi_{41} + 5\psi_{61}) + \tilde{R}_1^2(\psi_{40} + 6\psi_{60}) + \tilde{R}_2(2\psi_{40} + 4\psi_{60}),$$
$$\lambda_3 = \psi_{23} + \psi_{43} + \psi_{63} - \psi_{41} - 2\psi_{61} + \tilde{R}_1(2\psi_{22} + 4\psi_{42} + 6\psi_{62} - 2\psi_{40} - 8\psi_{60}) + \tilde{R}_1^2(3\psi_{41} + 10\psi_{61}) + \tilde{R}_1\tilde{R}_2(2\psi_{40} + 12\psi_{60}) + \tilde{R}_2(\psi_{21} + 3\psi_{41} + 5\psi_{61}) + \tilde{4}R_1^3\psi_{60} + \tilde{R}_3(2\psi_{40} + 4\psi_{60}),$$

under the truncation described in the text.

The condition (36b) is alternatively stated as:

$$-\hat{\alpha}(\bar{\psi} + \psi') + \tilde{b}' = 0,$$

at $r = R$. Here, the first two terms above contain a common factor of $1 - \mu^2$. By comparing them with the expansion (35c), we conclude $b_{0m} = 0$ for all m. The remaining part reduces to Eq. (38b) with the parameters defined by

$$\hat{\alpha}B_0 = b_{20} + b_{40},$$
$$\hat{\alpha}B_1 = b_{21} + b_{41} + 2\tilde{R}_1 b_{40},$$
$$\hat{\alpha}B_2 = b_{22} - b_{40} + b_{42} + 2\tilde{R}_1 b_{21} + (\tilde{R}_1^2 + 2\tilde{R}_2)b_{40},$$
$$\hat{\alpha}B_3 = b_{23} - 2b_{40} + b_{43} + \tilde{R}_1(2b_{22} + 4b_{42} - b_{41}) + \tilde{R}_2(b_{21} + 3b_{41}) + 3\tilde{R}_1^2 b_{41} + 2(\tilde{R}_1\tilde{R}_2 + \tilde{R}_3)b_{40}.$$

The condition (36c) reduces to (38c) with the parameters defined by

$$\sigma_s = 1 + 2\tilde{R}_1\mu + 3\tilde{R}_2\mu^2 + 4\tilde{R}_3\mu^3,$$
$$\sigma_z = -\tilde{R}_1 + (1 - 2\tilde{R}_2)\mu + (2\tilde{R}_1 - 3\tilde{R}_3)\mu^2 + 3(\tilde{R}_2 - \tilde{R}_3)\mu^3 + O(\mu^4),$$
$$D_0 = 0, \quad D_1 = \frac{3}{2}\tilde{R}_1 \quad D_2 = 3\tilde{R}_1^2 \quad D_3 = (3 - 7\tilde{R}_1^2)\tilde{R}_1$$
$$E_0 = 0, \quad E_1 = 3\tilde{\beta} + \frac{\tilde{\gamma}}{7} - \frac{2}{7}, \quad E_2 = (\frac{5}{7}\tilde{\gamma} - 2)\tilde{R}_1, \quad E_3 = -5\tilde{\beta} + \frac{1}{7} + 2(\frac{5}{7}\tilde{\gamma} - 3)\tilde{R}_1 + (\frac{5}{7}\tilde{\gamma} - 2)\tilde{R}_2,$$
$$F_0 = \psi_{20} + 2\psi_{40} + 3\psi_{60}, \quad F_1 = \psi_{21} + 2\psi_{41} + 3\psi_{61} + 4\tilde{R}_1(\psi_{20} + 3\psi_{40} + 6\psi_{60}),$$
$$F_2 = \psi_{22} - 2\psi_{40} + 2\psi_{42} - 6\psi_{60} + 3\psi_{62} + \tilde{R}_1(5\psi_{21} + 14\psi_{41} + 27\psi_{62}) + \tilde{R}_1^2(-2\psi_{20} + 6\psi_{40} + 36\psi_{60}),$$
$$F_3 = \psi_{23} - 2\psi_{41} + 2\psi_{43} - 6\psi_{61} + 3\psi_{63} + \tilde{R}_1(6\psi_{22} - 12\psi_{40} + 16\psi_{42} - 48\psi_{60} + 30\psi_{62}) + \tilde{R}_1^2(14\psi_{41} + 54\psi_{61}) + \tilde{R}_1^3(\frac{20}{3}\psi_{20} - 8\psi_{60}),$$
$$G_0 = G_1 = 0, \quad G_2 = \frac{15}{2}\tilde{R}_1, \quad G_3 = \frac{15}{2}\tilde{R}_1^2,$$
$$H_0 = -\tilde{\beta} + \frac{\tilde{\gamma} - 1}{14}, \quad H_1 = (\frac{5}{14}\tilde{\gamma} - \frac{1}{2})\tilde{R}_1, \quad H_2 = 5\tilde{\beta} - \frac{1}{7} - (\frac{10}{7}\tilde{\gamma} + \frac{1}{2})\tilde{R}_1^2, \quad H_3 = -\tilde{R}_1 + \frac{1}{3}(\frac{5}{7}\tilde{\gamma} + \frac{1}{2})\tilde{R}_1^3,$$
$$K_0 = 0, \quad K_1 = \psi_{21} + \psi_{41} + \psi_{61}, \quad K_2 = 2(\psi_{22} + \psi_{42} + \psi_{62}) + \tilde{R}_1(5\psi_{21} + 7\psi_{41} + 9\psi_{61}),$$
$$K_3 = -3\psi_{23} - \psi_{41} + 3\psi_{43} - 2\psi_{61} + 3\psi_{63} + 4\tilde{R}_1(3\psi_{22} + 4\psi_{42} + 5\psi_{62}) + \tilde{R}_1^2(7\psi_{41} + 18\psi_{61}).$$

The three conditions at $O(\mu^0)$ from Eqs. (38a, b, c) are simply:

$$\psi_{20} + \psi_{40} + \psi_{60} = 0,$$
$$b_{20} + b_{40} = 0,$$
$$\psi_{20} + 2\psi_{40} + 3\psi_{60} = 0.$$

The next important constraints are found at $O(\mu^3)$ from (38a, b), which are: $\lambda_3 = O(\hat{\alpha}^2)$ and $B_3 = O(\hat{\alpha}^2)$. They lead to:

$$\tilde{f} = -\frac{7}{3}\tilde{A}\tilde{\psi}_{23} + O(\hat{\alpha}) = \frac{4}{13}\tilde{\tilde{b}}_{20} + O(\hat{\alpha}), \tag{A.2a}$$

where we have set $\psi_{nm} = \tilde{\alpha}\tilde{\psi}_{nm}$ and $b_{nm} = \tilde{\alpha}^2\tilde{\tilde{b}}_{nm}$. Consistency of the conditions (38a, b) at $O(\mu)$ leads to:

$$-\tilde{\psi}_{21} + \frac{3}{4}\tilde{\psi}_{23} = \frac{223}{32}\tilde{f} + O(\hat{\alpha}). \tag{A.2b}$$

Furthermore, consistency of the conditions (38a, c) at $O(\mu)$ leads to:

$$-\frac{5}{3}\tilde{\psi}_{21} + \frac{7}{4}\tilde{\psi}_{23} = \frac{1}{21} - \frac{49}{32}\tilde{f} + O(\hat{\alpha}). \tag{A.2c}$$

From Eqs. (A.2a, b, c), $\tilde{f}$, ψ_{21}, and , ψ_{23} are determined as (39a, b, c) to the leading order. Additionally, b_{20} is proved to be $O(\hat{\alpha}^2)$, as already suggested so that it does not appear in a final solution up to $O(\hat{\alpha})$. It also follows $b_{40} = O(\hat{\alpha}^2)$. Moreover, the condition (38b) at $O(\mu)$ leads to Eq. (39d), and it further substitution into (38b) at $O(\mu^2)$ leads to Eq. (39e).

Finally, the condition (38c) at $O(\mu^2)$ leads to:

$$\tilde{\psi}_{21} - \frac{3}{4}\tilde{\psi}_{23} = -\frac{95}{32}\tilde{f} + O(\hat{\alpha}), \tag{A.2d}$$

which directly contradicts with (A.2b). Thus, the expansion of the condition (38c) must be terminated at $O(\mu)$.

It is important to note the contradiction between (A.2b) and (A.2d) is not due to a finite truncation considered here. It can be shown that (A.2b) and (A.2d) are, respectively, more generally given by

$$\lambda_1 = -4\hat{\alpha}\tilde{f} + O(\hat{\alpha}^2), \tag{A.3a}$$

$$K_1 = O(\hat{\alpha}^2). \tag{A.3b}$$

At the same time, it can shown that

$$K_1 = \lambda_1 + O(\hat{\alpha}^2). \tag{A.3c}$$

Thus, these two conditions (A.3a, b) are not mutually compatible, and the attempt to establish the continuity of the tangent-component velocity must be terminated at $O(\mu)$. It suggests the limit of the similarity form assumed by Eqs. (29a, b).

References

Anders, E. H., D. Lecoanet, and B. P. Brown, 2019: Entropy rain: Dilution and compression of thermals in stratified domains. *Astrophysical Journal*, **884**,65. doi.org/10.3857/1538-4357/ab3644.

Bechtold, P., E. Bazile, F. Guichard, P. Mascart, and E. Richard, 2001: A mass-flux convection scheme for regional and global models. *Quator. J. Roy. Meteor. Soc.*, **127**, 869 –889.

Boyd, J. P., and H. Ma, 1990: Numerical study of elliptical modons using a spectrum method. *J. Fluid Mech.*, **221**, 597–611.

Chang, C., and S. G. Llewellyn Smith, 2018: The motion of a buoyancy vortex filament. *J. Fluid Mech.*, **857**, R1.

Chang, C., and S. G. Llewellyn Smith, 2020: Axisymmetric contour dynamics for buoyancy vortex rings. *J. Fluid Mech.*, **887**, A–28.

de Roode, S. R., A. P. Siebesma, H. J. J. Jonker, and Y. de Voogd, 2012: Parameterization of the vertical velocity equation for shallow cumulus clouds. *Mon. Wea. Rev.*, **140**, 2424–2436.

Flierl, G. R., 1987: Isolated eddy models in geophysics. *Ann. Rev. Fluid Mech.*, **19**, 493-530.

Fraenkel, L. E., 1972: Examples of steady vortex rings of small cross–section in an ideal fluid. *J. Fluid Mech.*, **51**, 118–135.

Haman, K. E., and S. P. Malinowski, 1989: Drag effects in convective drafts. *Atmos. Res.*, **24**, 325–331.

Hernandez-Deckers, D., S. C. Sherwood, 2016: A numerical investigation of cumulus thermals. *J. Atmos. Sci.*, **73**, 4117–4136.

Hicks, W. M., 1884: On the steady motion and small vibrations of a hollow vortex. *Phil. Trans. R. Soc. Lond. A*, **175**, 161–195.

Hill, M. J. M., 1894: On a spherical vortex. *Phil. Trans. Roy. Soc. A*, **185**, 213–245.

Lai, A. C. H., B. Zhao, A. W.–K. Law, and E. E. Adams, 2015: A numerical and analytical study of the effect of aspect ratio on the behaviorof a round thermal. *Environ. Fluid Mech.*, **15**, 85–108.

Lamb, H., 1932: *Hydrodynamics*, Cambridge University Press, Cambridge, 738pp.

Lecoanet, D., and N. Jeevanjee, 2019: Entrainment in resolved, dry thermals. *J. Atmos. Sci.*, **76**, 3785-3801.

Lundgren, T. S., and N. N. Mansour, 1991: Vortex ring bubbles. *J. Fluid Mech.*, **224**, 177–196.

McKim, B., N. Jeevanjee, and D. Lecoanet, 2020: Buoyant-driven entrainment in dry thermals. *Quator. J. Roy. Meteor. Soc.*, **146**, 415–425.

Morrison, H., 2016a: Impacts of updraft size and dimensionality on the perturbation pressure and vertical velocity in cumulus Convection. Part I: Simple, generalize analytic solutions. *J. Atmos. Sci.*, **73**, 1441–1454, https://doi.org/10.1175/JAS-D-15-0040.1.

Morrison, H., 2016b: Impacts of updraft size and dimensionality on the perturbation pressure and vertical velocity in cumulus convection. Part II: Comparison of theoretical and numerical solutions and fully dynamical simulations. *J. Atmos. Sci.*, **73**, 1455–1480, https://doi.org/10.1175/JAS-D-15-0041.1.

Morrison, H., and J. M. Peters, 2018: Theoretical expressions for the ascent rate of moist deep convective thermals. *J. Atmos. Sci.*, **75**, 1699-1719.

Morrison, H., N. Jeenvanjee, and J.–I. Yano, 2022: Dynamic pressure drag on rising buoyant thermals in a neutrally stable environment. *J. Atmos. Sci.*, **79**, 3045–3063.

Morton, B.R., G.I. Taylor, and J.S. Turner, 1956: Turbulent gravitational convection from maintained and instantaneous sources. *Proc. Roy. Soc. London*, **A234**, 1–23.

Norbury, J., 1972: A steady vortex ring close to Hill's spherical vortex. *Proc. Camb. Phil. Soc.*, **72**, 253–284.

Norbury, J., 1973: A family of steady vortex rings. *J. Fluid Mech.*, **57**, 417–431.

Pedley, T. J., 1968: The troidal bubble. *J. Fluid Mech.*, **32**, 97–112.

Pedlosky, J., 1987: *Geophysical Fluid Dynamics*, 2nd ed., Springer.

Romps, D. M., and A. B. Charn, 2015: Sticky thermals: Evidence for a dominant balance between buoyancy and drag in cloud updrafts. *J. Atmos. Sci.*, **72**, 2890-2901.

Scorer, R. S., 1957: Experiments on convection of isolated masses of buoyant fluid. *J. Fluid Mech.*, **2**, 583–594.

Simpson, J. S., and V. Wiggert, 1969: Models of precipitating cumulus towers. *Mon. Wea. Rev.*, **97**, 471–489.

Sherwood, S. C., D. Herandez-Decekrs, M. Colin, and F. Robinson, 2013: Slippery thermal and the cumulus entrainment paradox. *J. Atmos. Sci.*, **70**, 2426-2442.

Sullivan, I. S., J. J. Niemela, R. E. Hershberger, D. Bolster, and R. J. Donnelly, 2008: Dynamics of thin vortex rings. *J. Fluid Mech.*, **609**, 319–347.

Tarshish, N., N. Jeevanjee, and D. Lecoanet, 2018: Buoyant motion of a turbulent thermal, *J. Atmos. Sci.*, **75**, 3233-3244.

Turner, J. S., 1957: Bouyant vortex rings. *Proc. Roy. Soc. Lond.*, **A 239**, 61-75.

Vasel–Be–Hagh, A. R., R. Carriveau, and D. S.–K. Ting, 2015: A balloon bursting underwater. *J. Fluid Mech.*, **769**, 522–540.

Walters, J. K., and J. F. Davidson, 1963: The initial motion of a gas bubble formed in an inviscid liquid. part 2. The three–dimensional bubble and the toroidal bubble. *J. Fluid Mech.*, **17**, 321–336.

Yano, J.-I., 2014: Basic Convective Element: Bubble or Plume?: A Historical Review. *Atmos. Phys. Chem.*, **14**, 7019–7030. doi:10.5194/acp-14-7019-2014

Yano, J.-I., 2023: Similarity solutions of thermal vortex rings: Vorticity–dynamics based derivation. *AIP Advances*, **13**, 045123. DOI: 10.1063/5.0129309 https://pubs.aip.org/aip/adv/article/13/4/045123/2884961/Similarity-solutions-of-thermal-vortex-rings

Yano, J.–I., and H. Morrison, 2024: Thermal vortex ring: Vortex–dynamics analysis of a high–resolution simulation. *J. Fluid Mech.*, **991**, A18. doi:10.1017/jfm.2024.485.

Zhao, B., A. W. K. Law, A. C. H. Lai, and E. E. Adams, 2013: On the internal velocity and density structures of miscible thermals. *J. Fluid Mech.*, **722**, R5.

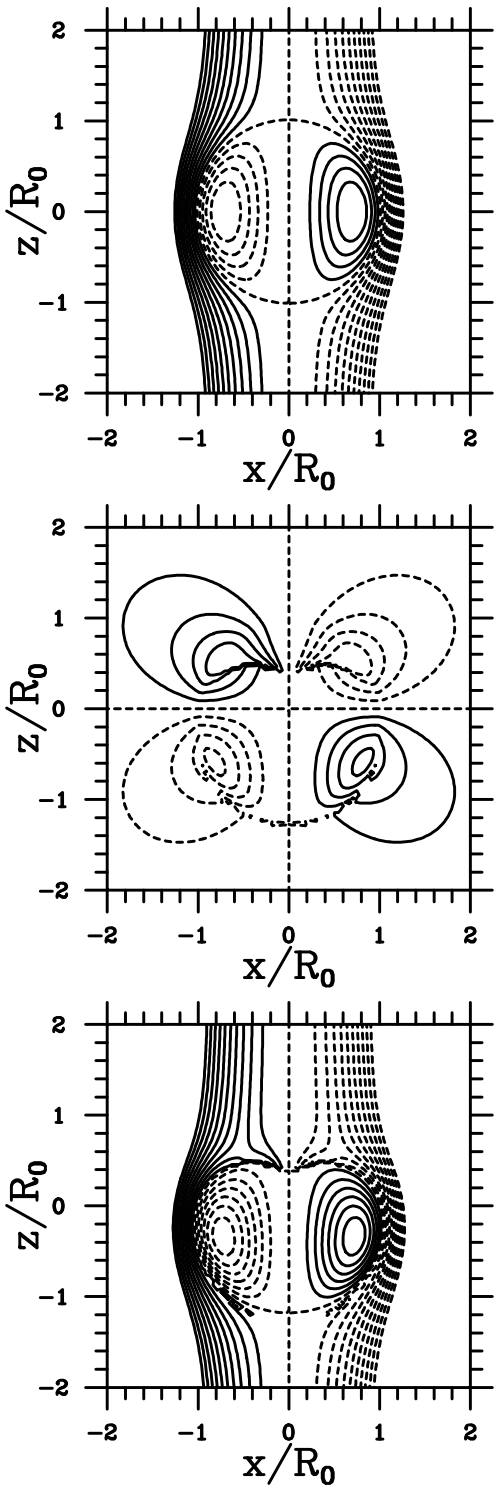

Figure 1. Streamfunctions of the steadily–propagating thermal vortex–ring solution. Top: leading–order solution (Hill's vortex), $\bar{\psi}$, defined by (2.13a); Middle: perturbation due to the buoyancy, ψ', defined by (18); Bottom: total, $\psi = \bar{\psi} + \psi'$. Here, the signs are defined as would appear on the x–z plane for the range of -0.02–0.02 with an interval of 0.005 and negative values indicated by dashed lines, with $R_0 = 1$, $c = 2/15$, $A = -1/5$, and $\hat{\alpha} = 1$.

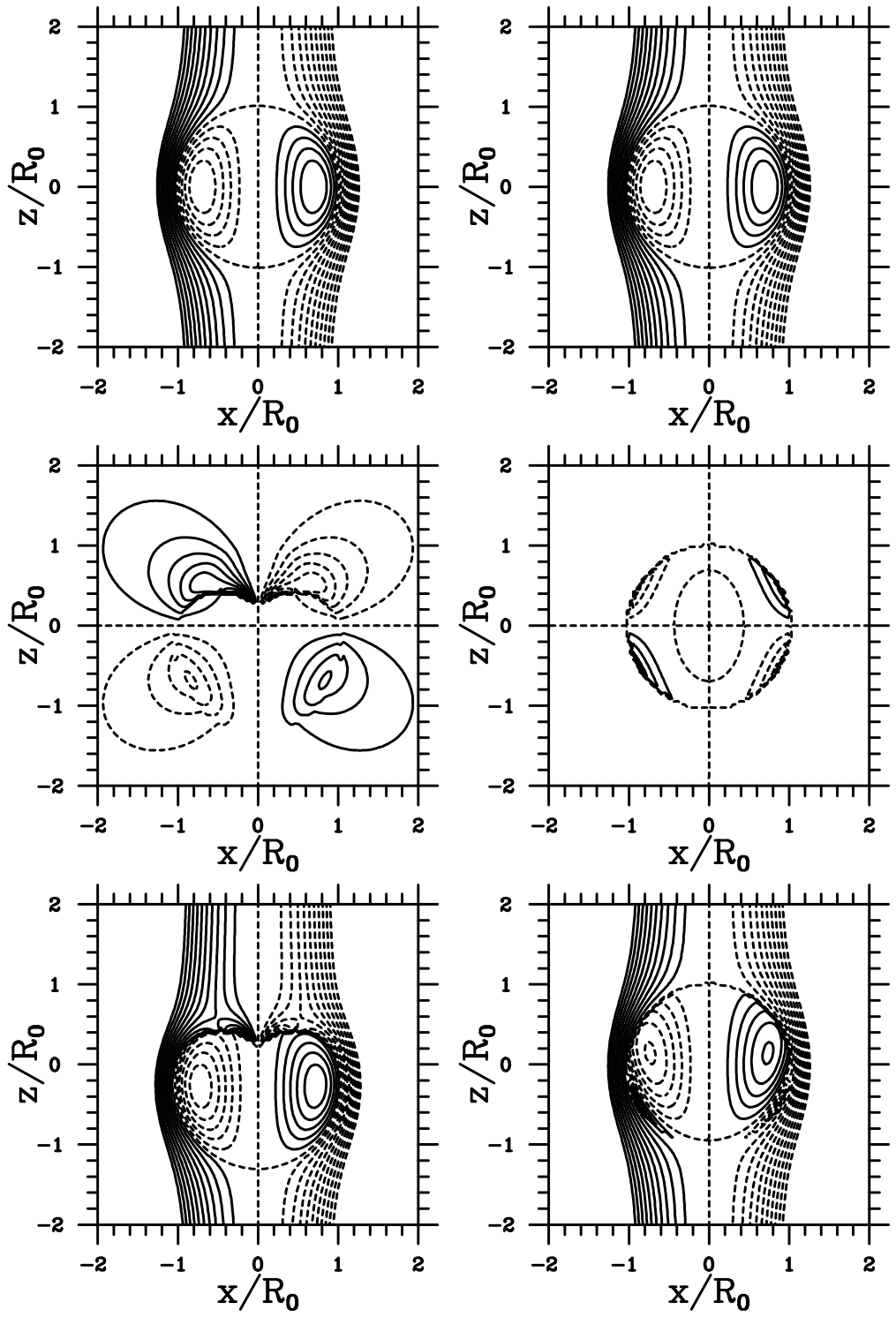

(a) The first mode with $\hat{\alpha} = 0.3$. (b) The second mode with $\hat{\alpha} = 1$.

Figure 2. Streamfunctions for the two nonlinear eigenmodes, in left and right, respectively, with the signs defined as would appear on the x–z plane for the range of -0.02–0.02 with an interval of 0.005 and negative values indicated by dashed lines, with $R_0 = 1$, $c = 2/15$, and $A = -1/5$. From top to bottom: $\bar{\psi}$, $\psi' + \tilde{\psi}'$, and the total ψ.

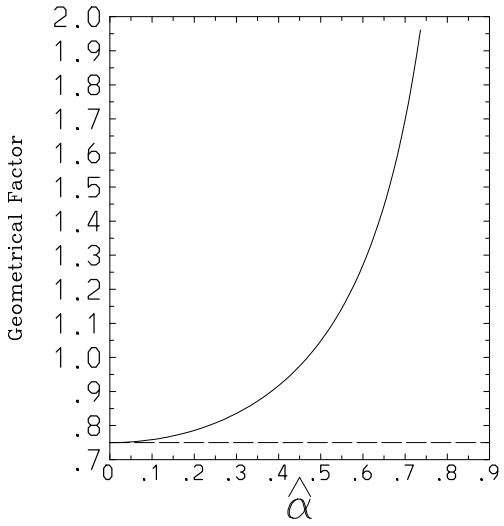

Figure 3. The geometrical factor, Γ, as a function of the nondimensional parameter, $\hat{\alpha} = \alpha R_0/Q_0 = 2\alpha R_0^3/15c$, which measures a relative contribution of the buoyancy to the vortex dynamics for the first (solid) and second (long dash) modes. Here, the geometrical factor is defined by $\Gamma = \pi R_0^3/V$ with V the volume of the vortex ring. Note that the value for the second mode remains very close to that for the sphere (3/4).

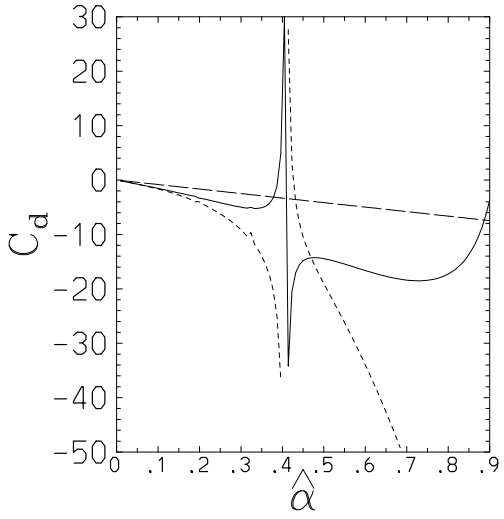

Figure 4. The dynamic pressure drag, C_d, as a function of the nondimensional parameter, $\hat{\alpha}$, which measures the relative contribution of the buoyancy to the vortex dynamics: for the first (solid) and second (long dash) modes. Furthermore, the evaluation based on the pressure gradient at $R \to \infty$ is shown by a short–dashed curve for the first mode. The curve for the second mode remains identical with the evaluation over the vortex–ring boundary.

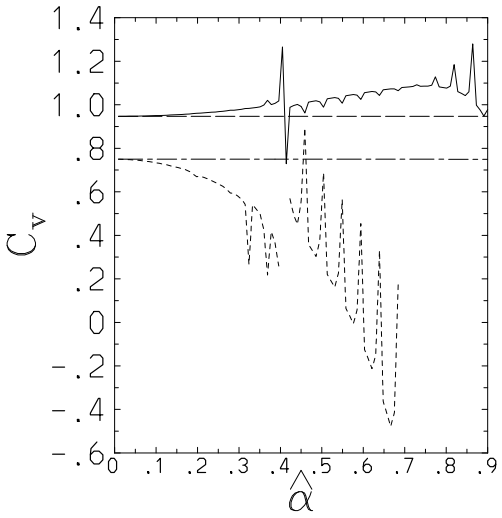

Figure 5. The virtual mass coefficient, C_v, which may be considered a nondimensional effective buoyancy, as a function of the nondimensional parameter, $\hat{\alpha} = 2\alpha R_0^3/15c$, which measures a relative contribution of the buoyancy to the vortex dynamics. The results are obtained by truncating the expansion by Legendre functions at $n = 6$. Here, the buoyancy pressure is diagnosed only by using the basic–buoyancy pressure distribution, $\bar{b}$: for the first (solid) and second (long dash) modes. Discontinuities with the former are due to singularities of the curve. Furthermore, the evaluations based on the pressure gradient at $R \to \infty$ are also shown by short– and chain–dashed curves, respectively, for these two modes.